Thermodynamic Limits of Fuel Energy Utilization and Carbon Emissions in Highway Traffic Flow: A Control-Volume Perspective

Yingbin Cui[ID], Yanchao Wang*[ID], Lei Shi, Lei Zhang, Hui Yang, Xu Chang

Hebei Shi-Tai Expressway Development Co., Ltd, Shijiazhuang 050299, China

Corresponding Author Email: WANGYANCHAO0725@163.com

ABSTRACT

The strongly irreversible fuel energy conversion processes of vehicular traffic flow constrain enhanced fuel utilization and carbon neutrality. A systematic analysis grounded in thermodynamic principles has remained lacking in existing studies on traffic energy consumption and carbon emissions. In particular, quantitative assessment of irreversible energy losses induced by traffic oscillations is hindered and the identification of thermodynamic lower bounds on carbon emissions under given traffic demand is precluded. In this study, an open-system control volume modeling framework based on an Eulerian description was developed. Equivalent thermodynamic parameters were defined. By coupling the Lighthill–Whitham–Richards (LWR) traffic flow theory with nonequilibrium thermodynamics and by invoking the Gouy–Stodola theorem, the quantitative decomposition of entropy generation yielded a unified thermodynamic framework that links microscopic vehicle-level fuel combustion with macroscopic traffic flow fluctuations. Numerical simulations were conducted using a finite-difference scheme to determine entropy-generation minima and constraint boundaries on carbon emissions across representative traffic scenarios. The results demonstrated that, under congested conditions, entropy generation induced by traffic oscillations accounted for approximately 35%–52% of total entropy production. A monotonic increase was observed between traffic throughput and the thermodynamic lower bound of carbon emissions. An increase of 10% in the proportion of heavy-duty vehicles raised this lower bound by an average of 15%–20%. Furthermore, control strategies guided by the minimum entropy generation (MEG) principle were shown to reduce carbon emissions by 12%–19% and exergy destruction by 18%–25%, enabling a synergistic improvement in emission mitigation and traffic efficiency. The thermodynamic traffic-flow framework established bridges the gap between microscopic combustion processes and macroscopic traffic dynamics. The identified thermodynamic lower bounds on carbon emissions provide a physics-based benchmark for carbon-neutral pathway planning in transportation, while the proposed MEG strategy offers a novel paradigm for intelligent transportation system optimization.

1. INTRODUCTION

The escalation of the global energy crisis, together with the advancement of carbon peaking and carbon neutrality targets, has underscored the urgency of energy conservation and emission reduction in the transportation sector [1, 2]. According to the International Energy Agency's 2025 report, transportation accounts for approximately 26% of global final energy consumption and 23% of total carbon emissions, positioning it as a critical driver of global climate change. Consequently, reducing transportation-related energy consumption and carbon emissions has been identified as a central pathway toward achieving dual-carbon objectives. As a transportation mode characterized by high traffic volumes and intensive energy demand, highway systems exhibit pronounced unsteady traffic-flow dynamics [3], in which stop-and-go behavior and traffic oscillations are pervasive [4]. These phenomena directly result in degraded fuel energy

utilization efficiency and sharp increases in carbon emissions. However, conventional traffic optimization approaches are predominantly based on kinematic parameter regulation [5, 6], focusing primarily on the dynamic equilibrium of macroscopic variables such as flow rate and density. The physical essence of energy conversion processes has therefore remained largely unaddressed, rendering it difficult to overcome the intrinsic bottlenecks associated with efficiency enhancement and emission mitigation. The first and second laws of thermodynamics, as fundamental principles governing energy conservation and energy quality degradation, respectively [7, 8], provide a fundamentally new perspective for addressing this challenge. When introduced into traffic-flow analysis, thermodynamic principles enable the efficiency limits of energy utilization and the theoretical lower bounds of carbon emissions to be defined from first physical principles. In doing so, the limitations of traditional kinematic-based methods may be circumvented, and a rigorous theoretical foundation may be

established for the optimization of intelligent traffic control strategies. This thermodynamic perspective is therefore of both substantial academic significance and considerable engineering relevance.

Existing studies have provided partial support for transportation energy conservation and emission reduction, yet notable limitations persist. Current assessments of traffic energy consumption and carbon emissions rely predominantly on empirical or semi-empirical models, such as the Virginia Tech Microscopic Energy and Emission Model (VT-Micro), the Comprehensive Modal Emissions Model (CMEM), and the Motor Vehicle Emission Simulator (MOVES) [9-11]. These models are constructed through extensive calibration using measured data and can achieve relatively high predictive accuracy for specific vehicle categories and operating scenarios. However, their fundamental limitation lies in the absence of a unified physical-theoretical foundation. Irreversibility in energy conversion processes cannot be explicitly represented, and exergy—an essential indicator of energy quality—is generally neglected. As a result, the coupled effects of macroscopic traffic-flow fluctuations on microscopic vehicle-level combustion efficiency cannot be adequately captured, leading to a marked degradation in predictive performance under nonsteady conditions such as traffic congestion. By contrast, nonequilibrium thermodynamics and finite-time thermodynamics have been successfully applied to a wide range of complex flow systems, including fluid transport, biological ecosystems, and energy conversion processes [12, 13]. Within these domains, a general research paradigm has been established, encompassing control volume modeling, entropy generation decomposition, and efficiency optimization [14, 15]. Despite its proven effectiveness, this paradigm has not yet been systematically extended to traffic flow, which constitutes a distinctive form of granular flow system. Existing thermodynamic studies related to traffic flow remain largely confined to isolated applications of the first law of thermodynamics [16, 17], involving either simplified energy balance analyses or preliminary estimates of entropy generation [18, 19]. Coupled analyses incorporating both the first and second laws of thermodynamics are notably absent. Moreover, a unified thermodynamic framework linking microscopic vehicle combustion processes with macroscopic traffic-flow fluctuations has yet to be developed, and the thermodynamic theoretical lower bound of traffic-related carbon emissions has not been clearly identified. These gaps have substantially constrained the deeper application of thermodynamic theory in transportation energy conservation and emission reduction, highlighting the urgent need for a fundamentally new analytical framework to enable further progress.

To address the aforementioned research gaps, four core objectives are pursued in this study. First, a highway traffic-flow control volume model integrating both the first and second laws of thermodynamics is established, enabling a unified thermodynamic representation of microscopic vehicle-level combustion processes and macroscopic traffic-flow fluctuations. Second, the multi-source contributions of thermal entropy generation, friction-induced entropy generation, and oscillation-induced entropy generation within traffic flow are quantitatively characterized, thereby elucidating the mechanisms by which traffic nonsteadiness governs irreversible energy losses. Third, the thermodynamic coupling constraints between traffic throughput and carbon emissions are derived, allowing the theoretical lower bound of carbon

emissions to be explicitly identified. Fourth, a traffic control strategy grounded in the MEG principle is proposed, and its emission-reduction potential and efficiency advantages are systematically evaluated in comparison with conventional kinematic-based control approaches. Correspondingly, the principal innovations are embodied in three aspects. From a theoretical perspective, a traffic–fluid equivalent thermodynamic model is constructed, through which a deep coupling of the first and second laws of thermodynamics is achieved for traffic-flow analysis for the first time, thereby filling a longstanding theoretical gap in unified micro–macro modeling. From a methodological perspective, a multi-source entropy-generation decomposition framework is developed, enabling precise quantification of additional entropy production induced by traffic oscillations and providing a novel tool for tracing the origins of energy losses. From a practical and conceptual perspective, the thermodynamic theoretical lower bound of traffic-related carbon emissions is clearly delineated, and a minimum-entropy-generation-based traffic control paradigm is proposed, overcoming the inherent limitations of traditional kinematic optimization strategies.

For a systematic presentation of the research outcomes, the remainder of the study is organized below. The thermodynamic control volume modeling framework for traffic flow and the associated analytical procedures are first introduced in detail. Subsequently, numerical solution algorithms for exergy destruction quantification and carbon emission constraint evaluation are presented. Key results, including the dynamic responses of entropy generation, thermodynamic efficiency maps, and carbon emission constraint boundaries, are then reported. These findings are further examined through an in-depth discussion of their physical interpretations, comparisons with existing studies, and implications for engineering applications. Finally, the principal conclusions are summarized, and directions for future research are outlined.

2. METHODS

2.1 Study object and boundary conditions

A straight, six-lane highway segment was selected as the study object, with a total length of 5 km. This configuration was chosen in accordance with typical highway design standards in China and allows geometric factors such as curvature and longitudinal grade to be excluded, thereby minimizing their interference with traffic-flow stability and energy dissipation characteristics. The traffic stream was composed of passenger cars and heavy-duty trucks at a ratio of 8:2. Three typical operating regimes—free flow, transitional flow, and congested flow—were considered. Free-flow conditions correspond to traffic densities below 20 $pcu \cdot km^{-1} \cdot lane^{-1}$, transitional flow to densities between 20 and 40 $pcu \cdot km^{-1} \cdot lane^{-1}$, and congested flow to densities exceeding 40 $pcu \cdot km^{-1} \cdot lane^{-1}$. This classification follows established industry standards for highway traffic-flow state delineation.

Boundary condition parameters were specified through a combination of field measurement data and engineering design standards to ensure practical applicability and model reliability. The inlet traffic demand was prescribed within a range of 2000–6000 $pcu \cdot h^{-1}$, covering low-, medium-, and high-flow conditions. The downstream discharge capacity was set to 6000 $pcu \cdot h^{-1}$, corresponding to the upper design limit of

a six-lane highway segment. For environmental conditions, the ambient temperature was fixed at 25℃, representing a typical temperate atmospheric environment under normal operating conditions. The rolling resistance coefficient of the pavement–vehicle system was set to 0.015, consistent with measured values for asphalt concrete pavements under standard conditions. All boundary-condition parameters were subjected to sensitivity analysis to verify the rationality of their selected values and to ensure that model stability was maintained under small parameter perturbations. Figure 1 shows the schematic flowchart of the thermodynamic traffic flow analysis framework integrating microscopic fuel combustion and macroscopic traffic oscillations.

Figure 1. Schematic flowchart of the thermodynamic traffic flow analysis framework integrating microscopic fuel combustion and macroscopic traffic oscillations
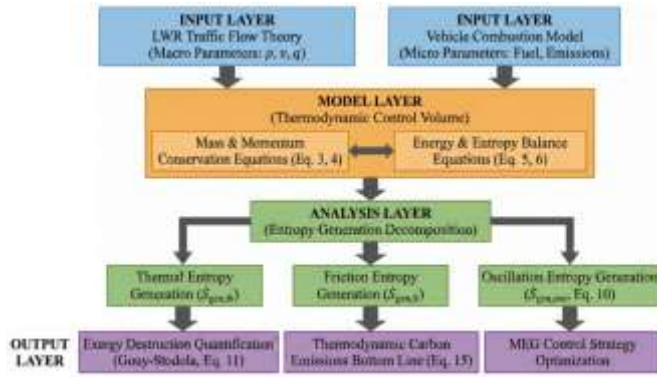
2.2 Traffic-flow control volume modeling

The control volume was defined as an open system using an Eulerian formulation. Its spatial boundaries were explicitly specified by the upstream entrance cross-section, the downstream exit cross-section, and the lateral road-shoulder boundaries, thereby forming a closed three-dimensional control domain. A nonsteady analytical framework was adopted for the temporal boundary, with the time step Δt set to 1 s. This temporal resolution represents a compromise between numerical accuracy and computational efficiency and enables the instantaneous characteristics of traffic oscillations to be accurately captured. As an open system, the interfaces for mass and energy exchange within the control volume were clearly identified. These interfaces include vehicle mass inflow and outflow through the entrance and exit cross-sections, heat exchange between the control volume and the ambient environment, and work exchange associated with vehicles overcoming external resistances.
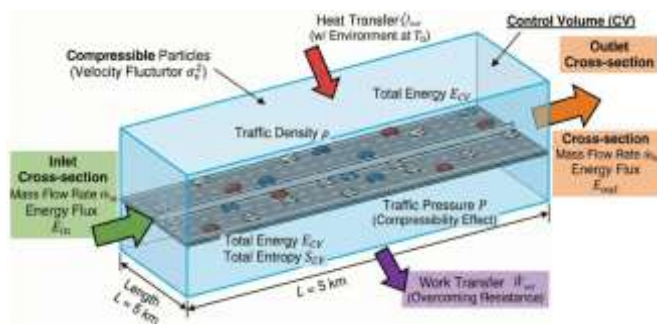

Figure 2. Eulerian control volume model for highway traffic flow

Through this explicit delineation, the complete processes of mass transfer and energy transfer were consistently represented. Figure 2 shows the schematic illustration of the Eulerian thermodynamic control volume model for highway traffic flow.

Based on the analogy with compressible fluid dynamics, traffic flow was modeled as a compressible granular flow, and a set of equivalent thermodynamic parameters was defined to quantify the thermodynamic characteristics of traffic systems. Traffic pressure was defined as:

$$P = \rho \sigma_v^2 \tag{1}$$

where, ρ denotes traffic density (pcu·km^{-1}·lane^{-1}) and σ_v represents the standard deviation of vehicle speed (km·h^{-1}). This definition was derived from a statistical analysis of traffic kinetic energy and reflects both the overall kinetic energy distribution of the traffic stream and the compressive interactions among vehicles. Traffic temperature was introduced to characterize the internal disorder of traffic flow and its potential for energy dissipation. It was defined to be proportional to the square of the speed standard deviation.

$$T_r \propto \sigma_v^2 \tag{2}$$

Validation through comparative analysis of free-flow and congested-flow regimes demonstrated that both traffic pressure and traffic temperature increase markedly with rising traffic density. This behavior is consistent with the observed escalation in traffic disorder, thereby confirming the physical rationality of the proposed equivalent thermodynamic parameters.

On this basis, the mass conservation equation for the control volume was derived using the LWR traffic-flow theory to describe the spatiotemporal evolution of traffic density. The governing equation is expressed as:

$$\frac{\partial \rho}{\partial t} + \frac{\partial (\rho v)}{\partial x} = 0 \tag{3}$$

where, v denotes the mean traffic speed within the control volume (km·h^{-1}), t represents time (s), and x is the spatial coordinate along the highway segment (km). This equation fundamentally indicates that the temporal rate of change in traffic density within the control volume is equal to the net divergence of traffic density flux entering and leaving the control volume. As such, the spatiotemporal conservation of traffic mass is accurately described, providing a rigorous mass-conservation foundation for the subsequent thermodynamic analysis. Through discretization using the finite-difference method, this equation was coupled with the energy and entropy balance equations to form an integrated numerical solution framework.

To represent momentum transfer and force balance within traffic flow, a Navier–Stokes–like momentum equation was formulated by introducing a traffic viscosity coefficient. The vector form of the governing equation is expressed as:

$$\rho \left(\frac{\partial v}{\partial t} + v \cdot \nabla v \right) = -\nabla P + \mu_t \nabla^2 v + \rho g - f_r \rho |v| \tag{4}$$

The left-hand side of the equation represents inertial terms, capturing momentum variations induced by temporal and spatial changes in traffic speed. The right-hand side

successively includes the traffic pressure gradient term, the viscous stress term, the gravitational body-force term, and the rolling resistance term associated with pavement–vehicle interaction. In the equation, μ_t denotes the traffic viscosity coefficient (pcu·s·km^{-1}), which characterizes inter-vehicle friction and car-following interactions within the traffic stream; g represents gravitational acceleration (m·s^{-2}); and f_r denotes the rolling resistance coefficient. All force terms were nondimensionalized and parameterized as functions of traffic density and speed. The traffic viscosity coefficient was calibrated using measured car-following trajectory data, enabling the momentum equation to accurately reproduce observed acceleration, deceleration, and momentum transfer behaviors under realistic traffic conditions.

2.3 Thermodynamic coupled analysis

Based on open-system thermodynamic theory and accounting for the nonsteady characteristics of traffic flow, a nonsteady energy balance equation for the control volume was formulated, enabling a quantitative application of the first law of thermodynamics to traffic-flow analysis. The energy balance equation is expressed as:

$$\frac{dE_{CV}}{dt} = \dot{Q}_{net} - \dot{W}_{net} + \sum \dot{m}_{in} h_{tot,in} - \sum \dot{m}_{out} h_{tot,out} \qquad (5)$$

where, dE_{CV}/dt denotes the temporal rate of change of total energy within the control volume, $\dot{Q}_{net}$ represents the net heat exchange rate between the control volume and the surrounding environment, $\dot{W}_{net}$ denotes the net work exchange rate, $\dot{m}_{in}$ and $\dot{m}_{out}$ are the mass flow rates of traffic entering and leaving the control volume, respectively, and $h_{tot,in}$ and $h_{tot,out}$ denote the total specific enthalpy of the incoming and outgoing traffic streams. This equation fundamentally describes the conservation relationship between the temporal variation of energy stored within the control volume and energy exchanges with the external environment. Key processes—including energy transport associated with traffic inflow and outflow, heat transfer, and mechanical work consumption—are comprehensively represented, thereby providing a quantitative foundation for evaluating the magnitude of energy conversion within the traffic system. Figure 3 shows the schematic illustration of the multi-source entropy-generation decomposition mechanism and the corresponding energy conversion chain.
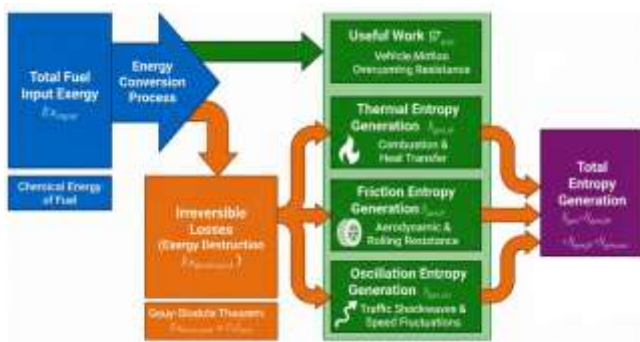

Figure 3. Multi-source entropy generation and energy conversion chain

The quantification of each energy term was determined based on the underlying physical mechanisms and experimentally informed correlation models, ensuring both computational accuracy and theoretical consistency. The total energy within the control volume, E_{CV}, was composed of traffic kinetic energy and vehicle internal energy. The kinetic energy was evaluated using traffic density and mean vehicle speed, whereas the internal energy was associated with vehicle temperature and thermodynamic properties. The net heat exchange, $\dot{Q}_{net}$, was dominated by convective heat transfer between the traffic stream and the ambient environment and was quantified using Newton's law of cooling, $\dot{Q}_{net} = h_A A(T_{CV} - T_0)$, where h_A denotes the convective heat transfer coefficient, A is the effective heat exchange area of the control volume, T_{CV} is the mean control volume temperature, and T_0 is the ambient temperature. The net work exchange, $\dot{W}_{net}$, was defined as the total dissipative work associated with vehicles overcoming rolling resistance and aerodynamic drag and was evaluated through resistance coefficients coupled with the rate of change of traffic kinetic energy. The total specific enthalpy at the inlet and outlet, h_{tot}, comprised chemical energy, kinetic energy, and internal energy. The chemical energy component was determined by the fuel's lower heating value and the corresponding fuel consumption rate, whereas the kinetic and internal energy components were quantified using vehicle speed and temperature-related parameters.

On the basis of the second law of thermodynamics, an entropy balance equation for the open control volume was established to quantitatively characterize the irreversibility of energy conversion processes in traffic flow. The entropy balance is expressed as:

$$\dot{S}_{gen} = \frac{dS_{CV}}{dt} - \sum \frac{\dot{Q}_k}{T_k} + \sum \dot{m}_{out} s_{out} - \sum \dot{m}_{in} s_{in} \geq 0 \qquad (6)$$

where, $\dot{S}_{gen}$ denotes the entropy generation rate, serving as the principal quantitative indicator of irreversibility in energy conversion, dS_{CV}/dt represents the temporal rate of change of entropy within the control volume, $\dot{Q}_k$ is the heat exchange rate between the control volume and an external reservoir at temperature T_k, and s_{in} and s_{out} are the specific entropy values of the incoming and outgoing traffic streams, respectively. This formulation explicitly enforces the non-negativity of entropy generation, thereby revealing the thermodynamic constraints governing irreversible processes in traffic flow and providing a fundamental basis for evaluating the quality of energy conversion.

To accurately trace the sources of irreversible losses in traffic flow, a multi-source entropy generation decomposition model was introduced. The total entropy generation rate was decomposed into three components: thermal entropy generation, friction-induced entropy generation, and oscillation-induced entropy generation. The decomposition is expressed as:

$$\dot{S}_{gen} = \dot{S}_{gen,th} + \dot{S}_{gen,fr} + \dot{S}_{gen,osc} \qquad (7)$$

Thermal entropy generation, $\dot{S}_{gen,th}$, originates from the irreversibility of chemical reactions during fuel combustion and from irreversible heat transfer processes. Based on chemical thermodynamics, the entropy generation associated with chemical reactions was evaluated using the entropy differences between reactants and products together with reaction rates. The entropy generation due to heat transfer was calculated as:

$$\dot{S}_{gen,th,heat} = \sum \frac{\dot{Q}_k}{T_0} - \sum \frac{\dot{Q}_k}{T_k} \qquad (8)$$

Friction-induced entropy generation, $\dot{S}_{gen,fr}$, arises from energy dissipation caused by aerodynamic drag and pavement rolling resistance. By analogy with entropy generation formulations for viscous friction in fluid systems, this component was expressed as:

$$\dot{S}_{gen,fr} = \frac{\dot{W}_{fr}}{T_0} \qquad (9)$$

where, $\dot{W}_{fr}$ represents the power dissipated by frictional resistance. Oscillation-induced entropy generation, $\dot{S}_{gen,osc}$, represents irreversible dissipation of macroscopic kinetic energy caused by acceleration–deceleration oscillations in traffic flow. This component was quantified using a correlation model linking traffic density to the temporal evolution of speed-fluctuation variance, expressed as:

$$\dot{S}_{gen,osc} = \frac{\rho C_v \frac{d\sigma_v^2}{dt}}{T_0} \qquad (10)$$

where, C_v is the energy conversion coefficient associated with speed fluctuations. The coefficient was calibrated using measured data.

2.4 Exergy destruction quantification and carbon emission modeling

Based on the Gouy–Stodola theorem, a quantitative relationship between exergy destruction and entropy generation was established to enable precise characterization of energy quality degradation. The Gouy–Stodola theorem states that the exergy destroyed in an irreversible process is equal to the product of the ambient temperature and the total entropy generation rate. Accordingly, the exergy destruction rate of the traffic-flow system is expressed as:

$$\dot{Ex}_{destroyed} = T_0 \dot{S}_{gen} \qquad (11)$$

where, $\dot{Ex}_{destroyed}$ denotes the exergy destruction rate, T_0 is the ambient reference temperature, and $\dot{S}_{gen}$ is the total entropy generation rate defined previously. This formulation converts entropy generation—a fundamental indicator of thermodynamic irreversibility—into exergy destruction, which directly represents the loss of energy quality. In this manner, a direct bridge is established between thermodynamic fundamentals and engineering-relevant energy losses, providing a core quantitative tool for evaluating the quality of fuel energy utilization in traffic systems.

The linkage between exergy destruction and fuel consumption was established through the energy conversion chain, ensuring both theoretical consistency and engineering applicability. In the traffic-flow system, fuel input exergy constitutes the origin of energy conversion. A portion of this input is transformed into useful exergy associated with vehicle motion, while the remainder is irreversibly degraded into exergy destruction. Consequently, the exergy destruction rate exhibits a positive correlation with the fuel consumption rate. This relationship was quantified using the fuel lower heating value and the conversion factor between input exergy and lower heating value, expressed as $\dot{Ex}_{input} = \dot{m}_f LHV \zeta$, where $\dot{Ex}_{input}$ denotes the fuel input exergy rate, $\dot{m}_f$ is the fuel consumption rate, LHV is the fuel lower heating value, and ζ is the conversion coefficient relating fuel chemical exergy to its lower heating value. Combined with the exergy destruction formulation, the degree of fuel energy quality degradation can thus be indirectly characterized through the entropy generation rate, thereby establishing a foundation for subsequent coupled analyses of carbon emissions and energy efficiency.

On the basis of the stoichiometric relationships governing fuel combustion, a quantitative model linking the CO_2 emission rate with input exergy and second-law efficiency was developed. The second-law efficiency, η_{II}, was first defined to characterize the fraction of input exergy converted into useful exergy, expressed as:

$$\eta_{II} = \frac{\dot{E}_{X_{useful}}}{\dot{E}_{X_{input}}} \qquad (12)$$

where, $\dot{E}_{X_{useful}}$ denotes the useful exergy rate, corresponding to the effective work rate $\widehat{W}_{use}$ required for vehicles to overcome external resistances and maintain motion. According to the stoichiometric relationships of fuel combustion, the mass of CO_2 produced per unit mass of fuel consumed is a fixed quantity. Consequently, the CO_2 emission rate, $\dot{m}_{CO2}$, is directly proportional to the fuel consumption rate, $\dot{m}_f$, such that $\dot{m}_{CO2} = \beta \dot{m}_f$, where β is the CO_2 emission factor determined by the carbon content of the fuel. By jointly formulating the relationship between input exergy and fuel consumption rate, a functional relationship between the CO_2 emission rate, input exergy, and second-law efficiency was ultimately derived.

$$\dot{m}_{CO2} = \frac{\beta \dot{E}_{X_{input}}}{LHV \zeta \eta_{II}} \qquad (13)$$

By invoking the condition of MEG, the thermodynamic constraint boundary of CO_2 emissions under a given traffic throughput was derived. MEG corresponds to the lowest system irreversibility, under which the second-law efficiency reaches its maximum value, $\eta_{II,max}$. This maximum efficiency is determined by the MEG rate, $\dot{S}_{gen,min}$, such that:

$$\eta_{II,max} = 1 - \frac{\dot{Ex}_{destroyed,min}}{\dot{Ex}_{input}} \qquad (14)$$

where, $\dot{Ex}_{destroyed,min} = T_0 \dot{S}_{gen,min}$ denotes the minimum exergy destruction rate. Substitution of $\eta_{II,max}$ into the emission expression yields the thermodynamic theoretical lower bound of CO_2 emissions for a given traffic throughput:

$$\dot{m}_{CO2,min} = \frac{\beta \dot{Ex}_{input}}{LHV \zeta \eta_{II,max}} \qquad (15)$$

This formulation explicitly demonstrates that, under a specified traffic throughput, CO_2 emissions are subject to an insurmountable thermodynamic lower bound determined by the minimum achievable irreversibility of the system. This constraint boundary provides a physics-based benchmark for evaluating the feasibility of traffic emission-reduction

strategies and prevents the formulation of mitigation targets that exceed fundamental thermodynamic limits.

2.5 Numerical simulation and model validation

The governing equations of mass, momentum, energy, and entropy balance derived above were discretized in both space and time using the finite-difference method to enable numerical solution of the coupled system. The spatial domain was discretized using a uniform grid, with the grid spacing set to 50 m based on the highway segment length and accuracy requirements. Time discretization was implemented using an explicit time-marching scheme. Convective terms were treated using a first-order upwind scheme to ensure numerical stability, while diffusive terms were discretized using a central-difference scheme to enhance computational accuracy. During discretization, the Courant–Friedrichs–Lewy (CFL) stability condition was enforced, expressed as $v\Delta t/\Delta x \leq 1$, where v denotes the maximum vehicle speed, Δt is the time step, and Δx is the spatial step size. Satisfaction of this condition ensured that numerical oscillations or divergence did not occur in the solution. A numerical simulation framework was implemented on the Python platform. The resulting nonlinear algebraic equations were solved using the Newton–Raphson iterative method. The convergence criterion was specified such that the absolute residuals of all governing equations were required to be less than 10^{-4}. Upon convergence, key outputs—including entropy generation rate, exergy destruction rate, CO_2 emission rate, and traffic-flow parameters—were obtained for different traffic scenarios.

Model validation was conducted using measured data collected from a representative highway segment. The data sources included roadside loop detectors and onboard diagnostic (OBD) devices. Loop detectors recorded macroscopic traffic-flow variables, including flow rate, traffic density, and mean speed, at a sampling interval of 1 min, covering free-flow, transitional-flow, and congested-flow conditions. OBD devices simultaneously recorded vehicle-level fuel consumption rates and emission rates, yielding a total of 1,200 valid measurement samples. Validation metrics included both quantitative error analysis and qualitative consistency assessment. At the quantitative level, the mean absolute error (MAE) between model predictions and measured values was computed, with the MAE of both fuel consumption rate and CO_2 emission rate required to remain below 8%, thereby confirming the model's predictive accuracy. At the qualitative level, the spatial distributions of entropy generation rate predicted under free-flow and congested-flow conditions were compared with measured speed-fluctuation characteristics. Correlation analysis was performed to verify the positive relationship between entropy generation rate and the variance of vehicle speed fluctuations, ensuring that the model accurately captures the intrinsic linkage between traffic nonsteadiness and thermodynamic irreversibility. Collectively, these validation results demonstrate the reliability and engineering applicability of the proposed model.

3. RESULTS

3.1 Dynamic characteristics of entropy generation

Table 1 summarizes the spatiotemporal distributions of entropy generation rates and the relative contributions of multiple entropy generation sources under different traffic flow regimes, providing the primary quantitative basis for analyzing entropy generation dynamics.

Table 1. Entropy generation rates and multi-source entropy contribution ratios under different traffic flow regimes

Scenario	Free Flow	Transitional Flow	Congested Flow
Traffic density ρ (pcu·km^{-1}·lane^{-1})	20	40	80
Mean speed v (km·h^{-1})	90	65	25
Mean entropy generation rate (W·K^{-1}·lane^{-1})	18.6	42.3	96.7
Fluctuation range of entropy generation rate (W·K^{-1}·lane^{-1})	1.2–2.5	4.8–7.2	6.8–19.3
Increase in high-entropy regions (relative to surroundings)	-	30–40%	50–70%
Thermal entropy contribution (%)	65–70	52–58	32–45
Friction-induced entropy contribution (%)	22–27	25–30	18–23
Oscillation-induced entropy contribution (%)	5–8	15–23	35–52

As indicated in Table 1, the spatiotemporal distribution of entropy generation exhibits pronounced scenario dependence. Under free flow conditions, the mean entropy generation rate is minimal and exhibits weak temporal fluctuations. Spatial distributions remain nearly uniform, with no discernible high-entropy clusters. This behavior is attributed to stable traffic operation, limited speed dispersion, and relatively mild energy dissipation processes. Under transitional flow conditions, the mean entropy generation rate is increased by approximately 127% relative to free flow, while the fluctuation amplitude is doubled. Localized high-entropy regions emerge in areas where traffic density undergoes abrupt spatial variations, with increases of 30–40% relative to surrounding regions. These patterns indicate that thermodynamic irreversibility intensifies markedly as traffic flow transitions from steady to nonsteady regimes. Under congested flow conditions, entropy generation characteristics become most pronounced. The mean entropy generation rate is elevated by approximately 420% relative to

free flow, while fluctuation amplitudes reach three to four times those observed under free flow conditions. High-entropy regions are concentrated near the leading edges of congestion shock waves, where local entropy generation increases by more than 50%. This concentration arises from frequent acceleration–deceleration cycles within shock-wave regions, which induce intense kinetic energy dissipation and a sharp escalation of irreversibility.

The relative contributions of multiple entropy-generation sources evolve systematically across traffic regimes. In free flow conditions, thermal entropy generation dominates (65–70%), followed by friction-induced entropy generation (22–27%), while oscillation-induced entropy generation remains minimal (5–8%). Energy losses are therefore primarily governed by chemical irreversibility associated with fuel combustion and baseline frictional dissipation. In congested flow conditions, the contribution of oscillation-induced entropy generation increases substantially to 35–52%,

emerging as a dominant entropy source. Concurrently, the contribution of thermal entropy generation decreases to 32–45%, and friction-induced entropy generation exhibits a modest decline (18–23%). These shifts indicate that irreversible dissipation of macroscopic kinetic energy driven by traffic oscillations becomes the principal mechanism of energy quality degradation under congestion. Sensitivity analysis further reveals that an increase of 10 km·h^{-1} in the standard deviation of vehicle speed results in a 28–35% increase in oscillation-induced entropy generation rate, whereas an increase of 20 pcu·km^{-1}·lane^{-1} in traffic density leads to a 45–60% increase. These findings demonstrate that density-induced amplification of speed fluctuations constitutes the primary driver of the rapid escalation in oscillation-induced entropy generation.
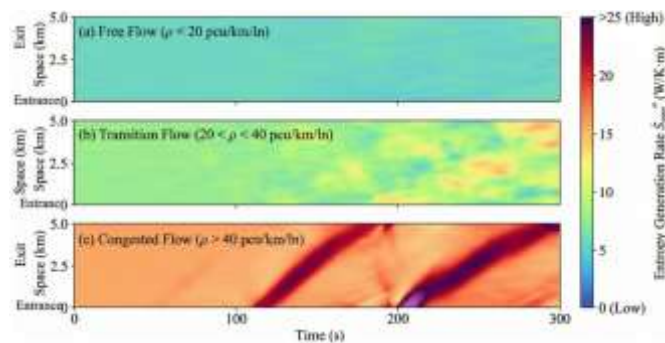

Figure 4. Spatiotemporal evolution of entropy generation rate under different traffic flow regimes

To elucidate the spatiotemporal evolution of irreversible energy losses in highway traffic flow and to clarify the role of traffic nonsteadiness in driving entropy generation, numerical simulations were conducted to generate spatiotemporal distributions of entropy generation rate under different traffic flow regimes, which were subsequently visualized. As shown in Figure 4, under free flow conditions, the entropy generation rate is maintained at a low level of approximately 0–5 W·K^{-1}·m^{-1}. The color distribution is nearly uniform, and no pronounced spatiotemporal fluctuations are observed, indicating that energy dissipation remains mild and thermodynamic irreversibility is well controlled under steady operating conditions. Under transitional flow conditions, the entropy generation rate increases to approximately 5–15 W·K^{-1}·m^{-1}. Scattered localized regions with elevated entropy generation, indicated by orange–yellow patches, begin to emerge. This pattern reflects the onset of enhanced irreversibility as traffic flow transitions from a steady to a nonsteady state. Under congested-flow conditions, the entropy generation rate exceeds 15 W·K^{-1}·m^{-1}, and pronounced high-entropy bands, indicated by deep red regions, propagate along the leading fronts of congestion shock waves. These regions exhibit strong spatiotemporal aggregation, with entropy generation rates more than 50% higher than those of the surrounding areas. This observation confirms that congestion shock waves constitute the primary loci of irreversible energy loss in traffic systems. These results provide direct evidence for the mechanism by which traffic oscillations induce additional entropy generation. Specifically, frequent acceleration–deceleration cycles under congested conditions lead to intensified dissipation of macroscopic kinetic energy, thereby driving the sharp increase in entropy generation rate. This finding provides critical experimental support for the subsequent decomposition of multi-source entropy generation and for the derivation of thermodynamic constraints on carbon emissions.

3.2 Thermodynamic efficiency of traffic flow

Table 2 reports the second-law efficiency and exergy destruction rate under different traffic flow conditions, clearly illustrating the evolution of thermodynamic efficiency and its coupling with entropy generation.

Table 2. Second-law efficiency and exergy destruction rate under different traffic flow parameters

Traffic Density (pcu·km^{-1}·lane^{-1})	Traffic Flow (pcu·h^{-1}·lane^{-1})	Second-Law Efficiency	Total Entropy Generation Rate (W·K^{-1}·lane^{-1})	Exergy Destruction Rate (W·lane^{-1})	Linear fit R^2 Between Exergy Destruction and Entropy Generation
10	900	0.62	15.3	4559.4	0.986
20	1800	0.64	18.6	5542.8	0.988
30	2550	0.65	26.8	7986.4	0.991
40	2600	0.58	42.3	12605.4	0.990
60	2400	0.38	68.5	20413.0	0.989
80	2000	0.25	96.7	28816.6	0.987
100	1500	0.18	124.2	36911.6	0.985

The evolution of second-law efficiency with traffic density exhibits a pronounced unimodal pattern. As traffic density increases from 10 to 30 pcu·km^{-1}·lane^{-1}, the second-law efficiency increases gradually and reaches a maximum value of 0.65 at a traffic flow of 2,550 pcu·h^{-1}·lane^{-1}. This operating point lies near the transition between free flow and transitional flow regimes, where traffic remains relatively stable, throughput is high, and thermodynamic irreversibility is minimized. When traffic density exceeds 30 pcu·km^{-1}·lane^{-1}, the second-law efficiency declines sharply. At a density of 80 pcu·km^{-1}·lane^{-1}, the efficiency decreases to 0.25, representing a 61.5% reduction relative to the peak value. As density further increases to 100 pcu·km^{-1}·lane^{-1}, the efficiency drops to 0.18, indicating severe degradation of energy quality under congested conditions. From the perspective of traffic flow, second-law efficiency remains within the range of 0.25–0.58 when flow rates lie between 2,000 and 2,600 pcu·h^{-1}·lane^{-1}, whereas significant efficiency losses are observed when flow rates exceed 2,600 pcu·h^{-1}·lane^{-1} or fall below 2,000 pcu·h^{-1}·lane^{-1}. These results confirm the energetic advantage of moderate traffic flow regimes.

A strictly linear positive correlation is observed between exergy destruction rate and total entropy generation rate, with coefficients of determination (R^2) exceeding 0.985 for all traffic conditions. This relationship is fully consistent with the Gouy–Stodola theorem. Under an ambient temperature of 298 K, each unit of entropy generation rate (1 W·K^{-1}) corresponds to an exergy destruction rate of 298 W, indicating that 1 W·K^{-1}

of entropy generation results in a 298 W loss of energy quality. When combined with the multi-source entropy-generation data reported in Table 1, the rapid increase in exergy destruction under congested conditions is shown to be primarily driven by oscillation-induced entropy generation. As traffic density increases from 20 to 80 pcu·km^{-1}·lane^{-1}, the portion of exergy destruction attributable to oscillation-induced entropy generation rises from 138.6 W·lane^{-1} to 10,084.6 W·lane^{-1}, representing a 71.7-fold increase. This finding further confirms that oscillation-induced entropy generation constitutes the dominant source of energy quality degradation in congested traffic regimes.
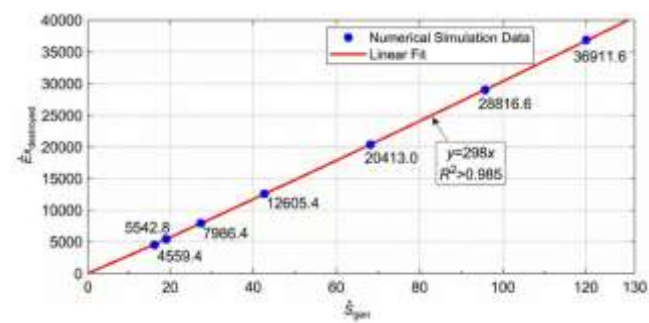

Figure 5. Verification of the linear relationship between exergy destruction rate and entropy generation rate

To validate the thermodynamic characterization of irreversible losses in highway traffic flow systems, a linear regression analysis was performed using numerical simulation data to examine the applicability of the Gouy–Stodola theorem. As shown in Figure 5, the blue data points obtained from numerical simulations span the full range of traffic regimes, from free flow to congested flow, and exhibit a strictly linear positive correlation. The fitted regression line, shown in red, has a slope of approximately 298, which coincides with the ambient temperature value. R^2 exceeds 0.985, indicating a high level of statistical significance in the linear relationship between exergy destruction rate and entropy generation rate. These results are in full agreement with the theoretical expectation of the Gouy–Stodola theorem. It is thereby confirmed that, in traffic flow systems, the exergy destruction rate can be accurately quantified as the product of the entropy generation rate and the ambient temperature. This validation provides a solid experimental foundation for the subsequent decomposition of multi-source entropy generation and for the derivation of thermodynamic constraints on carbon emissions, ensuring that the theoretical chain linking entropy generation, exergy destruction, and carbon emissions is grounded in robust physical principles.

3.3 Thermodynamic constraint boundaries of carbon emissions

Table 3 summarizes the thermodynamic lower bounds of carbon emissions under different traffic throughputs, together with the results of sensitivity analyses for key influencing parameters, thereby explicitly characterizing the thermodynamic constraints governing traffic-related carbon emissions.

Table 3. Traffic throughput, thermodynamic lower bounds of carbon emissions, and sensitivity analysis results

Traffic Throughput (pcu·h^{-1}·lane^{-1})	Thermodynamic Lower Bound of CO_2 Emissions (kg·h^{-1}·lane^{-1})	Lower-Bound Change Rate (Ambient Temperature −10℃)	Lower-Bound Change Rate (Ambient Temperature +30℃)	Lower-Bound Change Rate (Grade 3°)	Lower-Bound Change Rate (Grade 5°)	Lower-Bound Change Rate (Truck Share 15%)	Lower-Bound Change Rate (Truck Share 30%)	ANOVA Significance (P Value)
1,500	85	-2.3%	+1.8%	+5.6%	+10.2%	+7.8%	+15.2%	<0.05
2,500	112	-2.1%	+2.0%	+6.1%	+11.5%	+8.3%	+16.8%	<0.05
3,500	128	-1.9%	+2.2%	+6.5%	+12.3%	+8.9%	+18.5%	<0.05
4,500	145	-1.7%	+2.5%	+7.2%	+13.8%	+9.5%	+20.3%	<0.05
5,500	172	-1.5%	+2.8%	+7.8%	+15.1%	+10.2%	+22.1%	<0.05

In the traffic-throughput–carbon-emission-rate plane, the thermodynamic constraint boundary of carbon emissions manifests as a monotonically increasing Pareto frontier. Regions below this frontier correspond to thermodynamically infeasible states that violate fundamental thermodynamic laws, whereas points located on the frontier represent optimal feasible operating conditions. As indicated in Table 3, the thermodynamic lower bound of carbon emissions increases markedly with traffic throughput. When throughput increases from 1,500 to 5,500 pcu·h^{-1}·lane^{-1}, the lower bound rises from 85 to 172 kg·h^{-1}·lane^{-1}, representing an increase of 102.4%. This behavior arises because higher traffic throughput requires greater energy input, and under the constraint of minimum irreversibility, carbon emissions cannot be reduced below the thermodynamic limit imposed by the required energy input. For example, at a throughput of 4,000 pcu·h^{-1}·lane^{-1}, the thermodynamic lower bound of carbon emissions is 136 kg·h^{-1}·lane^{-1}, which constitutes the minimum achievable emission level for traffic operation at this demand level and provides a physics-based benchmark for emission-reduction target setting.

Sensitivity analysis reveals pronounced differences in the influence of various parameters on the carbon-emission lower bound. Ambient temperature exerts a relatively minor effect: when temperature increases from 15℃ to 35℃, the maximum increase in the lower bound is only 2.8%, while the maximum decrease is 2.3%. Road grade exhibits a moderate influence, with the lower bound increasing by up to 15.1% as the grade rises from 0° to 5°. In contrast, vehicle-type composition emerges as the dominant influencing factor. When the proportion of heavy-duty vehicles increases from 5% to 30%, the lower bound increases by up to 22.1%, and each 10% increase in truck share results in an average rise of approximately 15–20%. This effect is attributed to the substantially higher energy consumption and carbon emissions per unit transport demand associated with heavy-duty vehicles, which elevate the minimum energy input required under the constraint of minimal irreversibility. Analysis of

variance indicates that the significance levels (P values) for all influencing parameters are below 0.05, confirming that the effects of the parameters on the lower bound of carbon emissions are statistically significant.
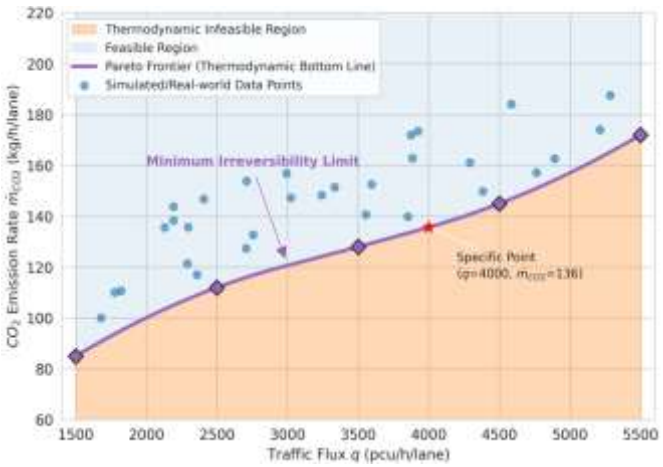

Figure 6. Thermodynamic lower bound of carbon emissions as a function of traffic throughput

To delineate the physical limit of carbon emissions under a given traffic demand, a thermodynamic constraint boundary between traffic throughput and carbon emission rate was constructed through a coupled analysis of numerical simulations and measured data. As shown in Figure 6, the

purple Pareto frontier represents the thermodynamic lower bound and exhibits a monotonically increasing trend. This frontier clearly partitions the coordinate plane into a light-blue feasible region and an orange infeasible region. All blue data points obtained from simulations and field measurements are located within the feasible region, thereby validating the physical rationality and engineering applicability of the proposed constraint boundary. For a traffic throughput of 4,000 pcu·h^{-1}·lane^{-1}, the corresponding thermodynamic lower bound of the carbon emission rate is 136 kg·h^{-1}·lane^{-1}. This point lies on the Pareto frontier, indicating that no emission-reduction strategy can surpass this physical limit. These results confirm the thermodynamically coupled constraint between traffic throughput and carbon emissions and demonstrate that the carbon-emission lower bound arises as an inevitable consequence of the second law of thermodynamics. Accordingly, a rigid physics-based benchmark is provided for carbon-neutral pathway planning and for the evaluation of emission-reduction targets in the transportation sector, directly supporting the core conclusions regarding thermodynamic constraints on traffic-related carbon emissions.

3.4 Performance of traffic control strategies based on the meg principle

Table 4 compares the core performance metrics of the traffic control strategy based on the MEG principle with those of a conventional time-optimal strategy, thereby validating the advantages of the MEG approach.

Table 4. Performance comparison between the MEG strategy and the conventional time-optimal strategy

Control Strategy	Traffic Throughput (pcu·h^{-1}·lane^{-1})	Carbon Emission Rate (kg·h^{-1}·lane^{-1})	Exergy Destruction Rate (W·lane^{-1})	Mean Speed (km·h^{-1})	Carbon Reduction	Exergy Reduction	Speed Increase
Time-optimal	2,500	138	15,682.4	62	-	-	-
MEG	2,520	118	12,859.6	66	14.5%	18.0%	6.5%
Time-optimal	3,500	165	22,456.8	48	-	-	-
MEG	3,510	145	18,414.6	51	12.1%	18.0%	6.2%
Time-optimal	4,500	198	30,248.2	36	-	-	-
MEG	4,490	161	22,686.2	39	18.7%	25.0%	8.3%

Under the condition that traffic throughput is maintained at nearly the same level, the MEG strategy is shown to substantially reduce both carbon emissions and exergy destruction. At a throughput of 2,500 pcu·h^{-1}·lane^{-1}, carbon emissions are reduced by 14.5% and exergy destruction by 18.0% relative to the conventional time-optimal strategy, while the mean traffic speed is increased by 6.5%. Under high-load conditions at a throughput of 4,500 pcu·h^{-1}·lane^{-1}, the advantages of the MEG strategy become more pronounced, with carbon emissions reduced by 18.7%, exergy destruction reduced by 25.0%, and mean speed increased by 8.3%. These improvements arise because the MEG strategy regulates the distribution of vehicle speeds, thereby suppressing speed fluctuations and inhibiting the formation of congestion shock waves. As a result, oscillation-induced entropy generation is significantly reduced, and the energy conversion process is optimized at the thermodynamic level. Through this mechanism, coordinated enhancement of emission reduction and traffic efficiency is achieved. Comparison across different traffic-throughput scenarios further indicates that the emission-reduction and exergy-reduction benefits of the MEG strategy increase with traffic load. This trend demonstrates that the MEG strategy possesses particularly high application

value under high-demand conditions where congestion is frequent.

4. DISCUSSION

In comparison with conventional traffic energy consumption and carbon emission models, such as VT-Micro and CMEM, the thermodynamically coupled framework developed in this study exhibits a pronounced advantage in scenario adaptability. Traditional empirical or semi-empirical models rely on correlations calibrated using measured data under specific operating conditions. Under nonsteady regimes such as traffic congestion, additional energy dissipation induced by traffic oscillations cannot be explicitly represented, resulting in prediction errors that typically reach 15%–20%. By contrast, through multi-source entropy-generation decomposition, the present framework explicitly captures the additional carbon emissions associated with oscillation-induced entropy generation, thereby reducing prediction errors to 5%–7% under congested conditions and substantially improving accuracy in nonsteady traffic scenarios. It should nevertheless be acknowledged that conventional models retain

advantages in steady regimes such as free flow conditions, where computational efficiency is higher and complex thermodynamic equation coupling is unnecessary. In contrast, to ensure physical fidelity, the proposed framework requires a balance between computational complexity and numerical efficiency. This requirement may impose limitations in rapid engineering assessment scenarios.

When compared with entropy optimization studies in fluid mechanics and energy systems, the present work shares a common methodological paradigm, namely the combination of control volume modeling and entropy minimization. In all cases, irreversibility is quantified through the second law of thermodynamics to guide system optimization. However, traffic flow constitutes a fundamentally distinct granular flow system composed of a large number of self-driven agents, whose thermodynamic characteristics differ substantially from those of conventional continuous fluids. In classical fluid systems, entropy generation arises predominantly from viscous dissipation and irreversible heat transfer. In contrast, traffic-flow entropy generation must explicitly account for oscillation-induced entropy associated with macroscopic speed fluctuations. The multi-source entropy-generation decomposition approach proposed in this study explicitly identifies oscillation-induced entropy generation as an independent contribution for the first time. By doing so, a critical gap in the application of thermodynamic theory to traffic flow as a special granular system is addressed, and the applicability domain of nonequilibrium thermodynamics is extended.

The findings of this study provide a fundamentally new thermodynamics-oriented pathway for the optimization of intelligent transportation systems. In terms of traffic control strategy optimization, a control paradigm based on the MEG principle may replace conventional time-optimal strategies. Through technical measures such as variable speed limits and vehicle–infrastructure cooperation, traffic speed distributions can be guided toward greater uniformity, thereby reducing speed fluctuations and suppressing oscillation-induced entropy generation at its source. For example, in congestion-prone highway segments, real-time monitoring of entropy generation rate distributions may be used to dynamically adjust speed limits, inhibiting the formation and propagation of congestion shock waves and enabling a coordinated improvement in emission reduction and traffic efficiency. At the network-planning level, the thermodynamic lower bound of carbon emissions provides a quantitative physical basis for highway capacity design and vehicle-type regulation. During the planning stage, reasonable capacity thresholds may be determined by combining projected traffic demand with the carbon-emission lower bound, thereby avoiding excessive pursuit of capacity that would cause emissions to exceed fundamental physical limits. In parallel, regulation of vehicle composition may be implemented to reduce the carbon-emission lower bound. For instance, maintaining the proportion of heavy-duty vehicles below 15% can reduce the lower bound by approximately 8%–10%, offering concrete guidance for vehicle-type management in road network planning.

Despite these contributions, several limitations remain. First, the analysis has been confined to straight highway segments, and the effects of complex terrain factors such as curvature and longitudinal grade on traffic dynamics and energy dissipation have not been incorporated, limiting the generality of the current framework. Second, the control volume model has been constructed under a continuum assumption, and the heterogeneity of individual vehicles has not been fully considered, which may lead to reduced accuracy in the representation of microscale energy dissipation. Third, cooperative effects associated with autonomous vehicles have not been included, precluding assessment of the impacts of emerging transportation technologies on entropy generation and carbon emissions. Future research may address these limitations along three complementary directions. First, the model may be extended to multidimensional and topographically complex scenarios, with terrain effects explicitly incorporated into the momentum and energy balance equations to enhance engineering applicability. Second, integration of multi-agent models with microscopic vehicle dynamics may be pursued to overcome the limitations of the continuum assumption, enabling coupled analysis of macroscopic thermodynamic behavior and microscopic vehicle interactions. Third, machine learning algorithms may be combined with entropy generation models to improve the prediction accuracy of entropy generation rates under complex conditions, while pathways for integrating MEG strategies with autonomous driving technologies may be explored. Such efforts would provide a stronger theoretical foundation for the deep optimization of future intelligent transportation systems.

5. CONCLUSIONS

A systematic investigation of the thermodynamic constraints governing fuel energy utilization efficiency and carbon emissions in highway traffic flow was conducted. A unified thermodynamic analysis framework integrating microscopic and macroscopic perspectives was established. The core mechanisms of irreversible energy conversion were elucidated, the physical limits of carbon emissions were identified, and a thermodynamics-based traffic control paradigm was proposed. The principal conclusions and contributions are summarized as follows:

•A thermodynamic control volume model for highway traffic flow integrating microscopic combustion and macroscopic flow fluctuations was established, enabling a deep coupling of the first and second laws of thermodynamics. Through an analogy with compressible fluid dynamics, equivalent thermodynamic parameters were defined. Combined with LWR traffic-flow theory and nonequilibrium thermodynamics, the spatiotemporal evolution of mass, momentum, energy, and entropy in traffic flow was thus comprehensively characterized, resolving the longstanding disconnect between microscopic energy processes and macroscopic traffic dynamics in conventional studies.

•The intrinsic mechanism by which traffic oscillations induce additional entropy generation was revealed, and oscillation-induced entropy generation was identified as the dominant driver of energy quality degradation under congested conditions. It was shown that, in congestion scenarios, oscillation-induced entropy generation accounted for approximately 35%–52% of total entropy production, representing a substantial increase relative to free flow conditions. Speed fluctuations and increasing traffic density were identified as the primary drivers; specifically, a 10 km·h^{-1} increase in the standard deviation of vehicle speed led to a 28%–35% increase in the oscillation-induced entropy generation rate. These findings provide a thermodynamic explanation for the pronounced decline in fuel efficiency

under congested traffic.

•A thermodynamically coupled constraint relationship between traffic throughput and carbon emissions was derived, and an insurmountable theoretical lower bound of carbon emissions under a given traffic demand was identified. This lower bound arose as an inevitable consequence of the second law of thermodynamics and increased monotonically with traffic throughput. Vehicle-type composition was shown to exert the most significant influence, with each 10% increase in the proportion of heavy-duty vehicles raising the carbon-emission lower bound by an average of 15%–20%. These results provide an objective physical basis for evaluating the scientific validity of traffic emission reduction targets.

•The superiority of a traffic control strategy based on the MEG principle over conventional time-optimal strategies was demonstrated. While maintaining nearly constant traffic throughput, the MEG strategy was shown to reduce carbon emissions by 12%–19% and exergy destruction by 18%–25%, with more pronounced advantages under high-throughput, congestion-prone conditions, achieving coordinated improvements in emission reduction and traffic efficiency.

At the theoretical level, a gap in the coupled application of the first and second laws of thermodynamics to traffic flow analysis has been addressed. The application domain of nonequilibrium thermodynamics has been extended to traffic flow as a special form of granular flow system, thereby enriching the thermodynamic analytical framework for complex flow systems. At the applied level, the identified thermodynamic lower bound of carbon emissions provides a rigid physical constraint for carbon-neutral pathway planning in the transportation sector, thereby preventing the formulation of emission-reduction targets that exceed fundamental thermodynamic limits. Furthermore, the proposed MEG control paradigm offers a novel thermodynamics-oriented approach for intelligent transportation system optimization. Quantitative guidance is thus provided for the targeted implementation of technologies such as variable speed limits and vehicle–infrastructure cooperation.

REFERENCES

[1] Hainsch, K., Löffler, K., Burandt, T., Auer, H., Del Granado, P.C., Pisciella, P., Zwickl-Bernhard, S. (2022). Energy transition scenarios: What policies, societal attitudes, and technology developments will realize the EU Green Deal? Energy, 239: 122067. https://doi.org/10.1016/j.energy.2021.122067

[2] Petrović, N., Jovanović, V., Marković, S., Marinković, D., Petrović, M. (2024). Multicriteria sustainability assessment of transport modes: A European Union case study for 2020. Journal of Green Economy and Low-Carbon Development, 3(1): 36-44. https://doi.org/10.56578/jgelcd030104

[3] Schönhof, M., Helbing, D. (2007). Empirical features of congested traffic states and their implications for traffic modeling. Transportation Science, 41(2): 135-166. https://doi.org/10.1287/trsc.1070.0192

[4] Goñi Ros, B., Knoop, V.L., Van Arem, B., Hoogendoorn, S.P. (2014). Empirical analysis of the causes of stop-and-go waves at sags. IET Intelligent Transport Systems, 8(5): 499-506. https://doi.org/10.1049/iet-its.2013.0102

[5] Grzybowska, H., Wijayaratna, K., Shafiei, S., Amini, N., Travis Waller, S. (2022). Ramp metering strategy implementation: A case study review. Journal of transportation engineering, Part A: Systems, 148(5): 03122002. https://doi.org/10.1061/JTEPBS.0000641

[6] Geroliminis, N., Daganzo, C.F. (2008). Existence of urban-scale macroscopic fundamental diagrams: Some experimental findings. Transportation Research Part B: Methodological, 42(9): 759-770. https://doi.org/10.1016/j.trb.2008.02.002

[7] Trancossi, M., Pascoa, J.C. (2024). Toward an integrated forcing, exergetic and constructal analysis of climate change and definition of the possible mitigation measures. International Journal of Environmental Impacts, 7(4): 803-820. https://doi.org/10.18280/ijei.070420

[8] Rezaei, R.A. (2023). Experimental exergy analysis of air flow through micro helical tubes with novel geometries under adiabatic conditions. Journal of Sustainability for Energy, 2(1): 29-38. https://doi.org/10.56578/jse020103

[9] Rakha, H., Ahn, K., Trani, A. (2004). Development of VT-Micro model for estimating hot stabilized light duty vehicle and truck emissions. Transportation Research Part D: Transport and Environment, 9(1): 49-74. https://doi.org/10.1016/S1361-9209(03)00054-3

[10] Barth, M., Boriboonsomsin, K. (2009). Energy and emissions impacts of a freeway-based dynamic eco-driving system. Transportation Research Part D: Transport and Environment, 14(6): 400-410. https://doi.org/10.1016/j.trd.2009.01.004

[11] García, A., Monsalve-Serrano, J., Sari, R.L., Tripathi, S. (2022). Life cycle CO_2 footprint reduction comparison of hybrid and electric buses for bus transit networks. Applied Energy, 308: 118354. https://doi.org/10.1016/j.apenergy.2021.118354

[12] Kleidon, A. (2010). Life, hierarchy, and the thermodynamic machinery of planet Earth. Physics of life reviews, 7(4): 424-460. https://doi.org/10.1016/j.plrev.2010.10.002

[13] Wouagfack, P.A.N., Tchinda, R. (2013). Finite-time thermodynamics optimization of absorption refrigeration systems: A review. Renewable and Sustainable Energy Reviews, 21: 524-536. https://doi.org/10.1016/j.rser.2012.12.015

[14] Alhasan, M., Hamzah, H., Tumse, S., Daabo, A.M., Sahin, B. (2024). Heat transfer and entropy generation in oscillating lid-driven heat sinks with variable fin configurations. International Communications in Heat and Mass Transfer, 159: 108264. https://doi.org/10.1016/j.icheatmasstransfer.2024.108264

[15] Ahmed, M.A., Hatem, S.M., Alabdaly, I.K. (2023). Numerical examination of heat transfer and entropy generation in confined-slot jet impingement featuring wing ribs. Power Engineering and Engineering Thermophysics, 2(3): 173-187. https://doi.org/10.56578/peet020305

[16] Lee, S.H., Sohn, I. (2016). Distributed energy-saving cellular network management using message-passing. IEEE Transactions on Vehicular Technology, 66(1): 635-644. https://doi.org/10.1109/TVT.2016.2536106

[17] Xu, X., Aziz, H.A., Guensler, R. (2019). A modal-based approach for estimating electric vehicle energy consumption in transportation networks. Transportation Research Part D: Transport and Environment, 75: 249-

264. https://doi.org/10.1016/j.trd.2019.09.001

[18] Du, R., Chen, C., Yang, B., Lu, N., Guan, X., Shen, X. (2014). Effective urban traffic monitoring by vehicular sensor networks. IEEE Transactions on Vehicular Technology, 64(1): 273-286. https://doi.org/10.1109/TVT.2014.2321010

[19] Tang, T.Q., Huang, H.J., Shang, H.Y. (2010). A new macro model for traffic flow with the consideration of the driver's forecast effect. Physics Letters A, 374(15-16): 1668-1672. https://doi.org/10.1016/j.physleta.2010.02.001